Chapter 3

Membranes

Figure 3.1 shows an example of a two-dimensional network in a cell. Shown is the membrane-associated cytoskeleton of the human erythrocyte. The image showes that there is a network of spectrin tetramers attached to cytoplasmic side of plasma membrane about midway along their length by the protein ankyrin. Each spectrin tetramer has a $200\ nm$ contour length with an end-to-end distance of $< R_e > \ 70\ nm$.

3.1 Self–assembly of micelles

3.1.1 Differential geometry of surfaces

We shall first be concerned with the intrinsic and extrinsic geometric properties of surfaces, such as the curvature. For simplicity we consider a surface S which is the graph of a function with continuous second derivatives. This may be of the form $z = f(x, y)$ or parameterized $f(s, t), g(s, t), h(s, t)$ for a two-dimensional surface embeded in three-dimensional space. Let $\mathbf{n}$ denote a unit normal vector to S at a point $\mathbf{p}$ choosen such that the normal vector is pointing along the z-axis. Now slice S by planes containing $\mathbf{n}$ and consider the curvature of the resulting curves. The curvatures of these resulting curves are called *normal curvatures* at $\mathbf{p}$. The maximum normal curvature κ_1 and the minimum normal curvature κ_2 are called *principal curvatures*. The *Gaussian curvature* $K(\mathbf{p})$ at any point p on S is the product of the extreme curvatures of the curves through $\mathbf{p}$ cut out by

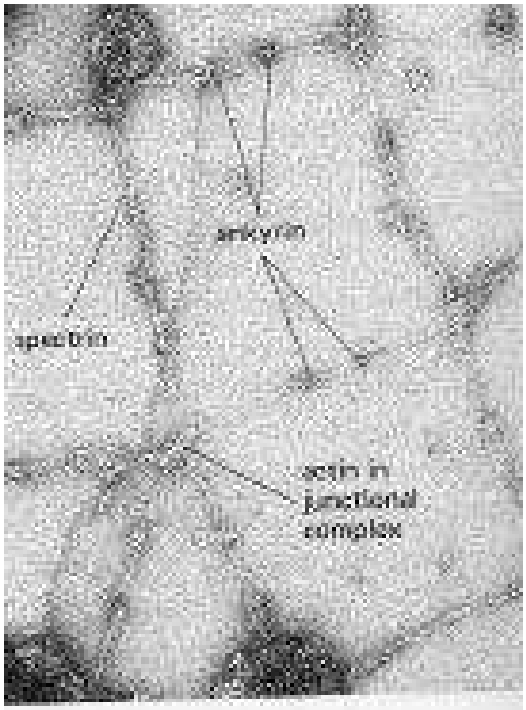

Figure 3.1: An example of a two-dimensional network in a cell taken from [110]

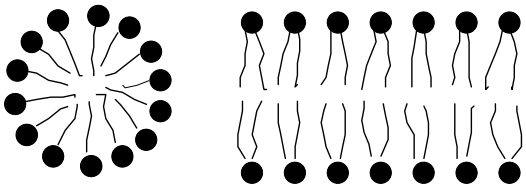

Figure 3.2:

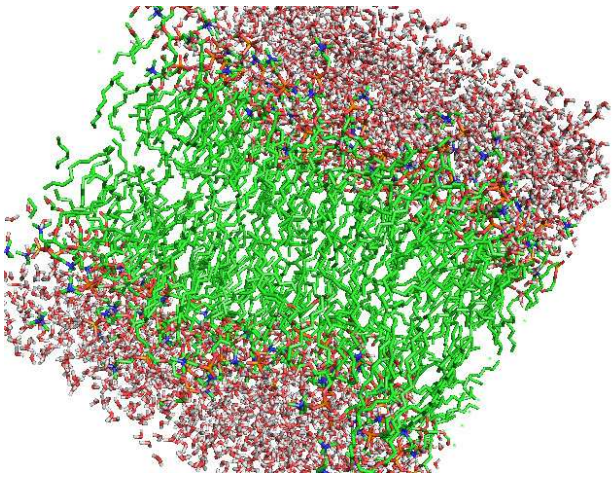

Figure 3.3:

normal planes (the product of the principal curvatures). The Gaussian curvature is a measure of how much "curvedness" the surface displays. We have to be careful. The curvature of a curve is an extrinsic geometric property, telling how it is bent in the plane, or bent in space. whereas the Gaussian curvature is an intrinsic geometric property: it stays the same no matter how a surface is bent, as long as it is not distorted, neither stretched or compressed. But the mean curvature

$$H = \frac{1}{2}(\kappa_1 + \kappa_2) \tag{3.1}$$

is an extrinsic property of the surface.

Example 3.1.1

Let us look at the monkey saddle (see als figure 3.4)

$$f(x, y) = z = x^3 - 3 * x * y^2 \tag{3.2}$$

The Gaussian curvature of the monkey saddle is given by

$$K = \frac{-36\,x^2 - 36\,y^2}{\left[1 + \left(3\,x^2 - 3\,y^2\right)^2 + 36\,x^2y^2\right]^2} \tag{3.3}$$

and the mean curvature by

$$H = -27\,\frac{x\left(x^4 - 2\,x^2y^2 - 3\,y^4\right)}{\left(1 + 9\,x^4 + 18\,x^2y^2 + 9\,y^4\right)^{3/2}} \tag{3.4}$$

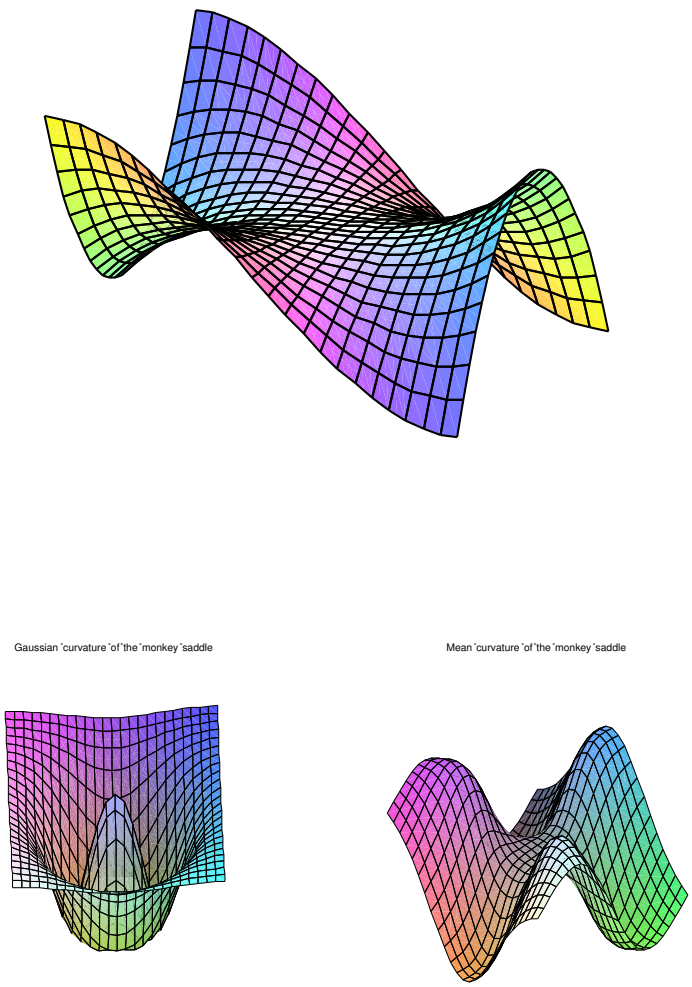

Figure 3.4: Shown is the monkey saddle and the corresponding curvatures.

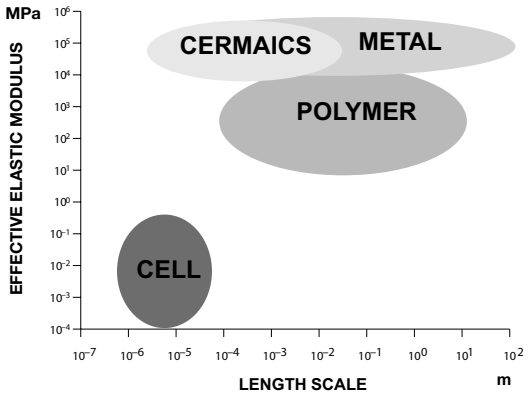

Figure 3.5: Comparison of the elastic modulus for different materials

3.1.2 Membrane elasticity and bending energy

Fluctuating membranes and surfaces are basic structural elements of biological systems and complex fluids. Recent theoretical work [158, 159] and experimental studies [160, 161] indicate, that these sheetlike macromolecules should have dramatically different properties than linear polymers. Polymerized membranes which contain a permanently cross-linked network of constituent molecules have a shear elasticity, giving them a large entropic bending rigidity.

A possible approach to study the behaviour of a surface in space dimensions $D > 1$ is to discretize the surface using a triangulation [111, 112, 113, 165]. This, in a sense, connects with the network shown in figure 3.1. Thus the basic idea is to replace the complex network with a simple model where the edges of the triangulation represent the membrane polymers (spectrin network) and are modelled by Hookian springs with a quadratic potential.

The surface S is thus replaced by a simplical triangulation T, specified by the number of nodes N, of links and triangles, and the X-coordinate field by the coordinates X of the nodes (see figure).

The metrical fluctuations of the manifold are modeled by summing over triangulations induced by link-flips [115, 116, 117]. The Hamiltonian is now choosen, such that the partition function is not dominated by configurations with spikes. In order to surpress these spikes one adds a term with extrinsic curvature.

As a function of the extrinsic curvature the model shows a transition (crumpling

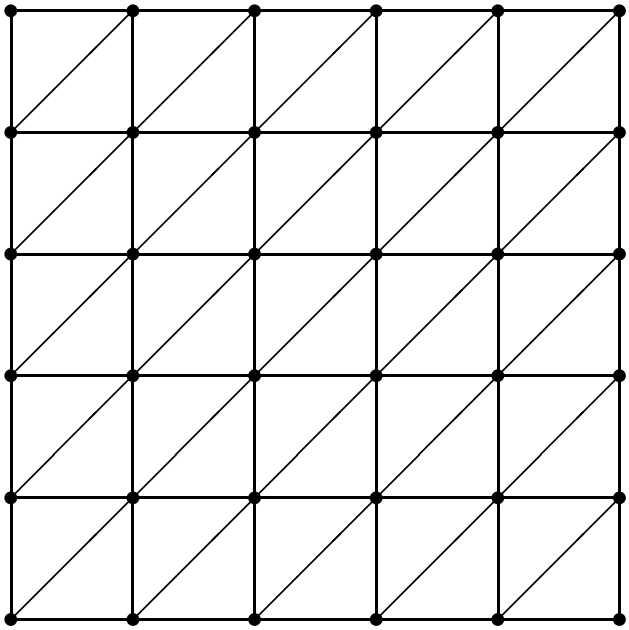

Figure 3.6:

transition) at finite rigidity of the surface [118, 119, 120, 121, 122, 123, 124, 125, 126, 127, 128].

The partition function can be written as

$$Z_N = \int d^D X_0 \int \prod_{i=1}^{N-1} d^D X_i e^{-H} \tag{3.5}$$

where the translational mode is integrated out. The Hamiltonian H is defined as

$$H = \underbrace{\beta \cdot \sum_{\langle i,j \rangle}^{N} (X_i^\mu - X_j^\mu)^2}_{\mathcal{H}_g} + \underbrace{\lambda \cdot \sum_{\triangle_i, \triangle_j} (1 - \hat{n}_{\triangle_i} \cdot \hat{n}_{\triangle_j})}_{\mathcal{H}_e} - \underbrace{\alpha \cdot \sum_{i=0}^{N} \log \sigma_i}_{\mathcal{H}_m} \quad . \tag{3.6}$$

The Gaussian part of the Hamiltonian H_g is a sum over the positions X in embedding Euclidian space of all nearest neighbours nodes, i.e. all links of the triangulation. We shall use $\beta = 1$ because of the rescaling invariance, i.e., if we rescale the coordiantes

$$X \to X' = \sqrt{\beta} X \tag{3.7}$$

then the partition function is replaced by

$$Z' = \beta^{(N-1)D/2} c \tag{3.8}$$

where c is a constant independent of β. If λ and α are both zero, then the we would obtain the average area $< A >$ as

$$< A >= -\frac{\partial \ln Z}{\partial \ln \beta} = \frac{D}{2}(N-1)\frac{1}{\beta} \tag{3.9}$$

and for the fluctuations

$$< A^2 > - < A >^2 = -\frac{\partial^2 \ln Z}{\partial^2 \ln \beta} = \frac{D}{2}(N-1)\frac{1}{\beta^2} \tag{3.10}$$

Hence the relative width of the distribution vanishes in the thermodynamic limit

$$\lim_{N\to\infty} \frac{\sqrt{< A^2 > - < A >^2}}{< A >} = \lim_{N\to\infty} \frac{1}{\sqrt{\frac{D}{2}(N-1)}} = 0 \tag{3.11}$$

H_e is an *edge extrinsic curvature* term [129, 130, 131, 132, 133, 134, 135, 136]. $\sum_{\triangle_i,\triangle_j}$ denotes a summation over all adjacent triangles which share an edge and $\hat{n}_{\triangle_i} \cdot \hat{n}_{\triangle_j}$ is the scalar product of the vectors normal to a triangle.
The third part of the Hamiltonian H_m is the discretization of the square root of the metric. σ_i denotes the number of nearest neighbours of node i. α depends on the measure. We will set $\alpha = D/2$ for the $D = 3$ dimensional embedding space.
We expect that the above model shows a phase transition at some critical value of the coupling λ. There are several questions which we want to address: What is the order of the transition? If the transition is of second order, what are the exponents? Are the exponents topology dependent? Is the transition temperature topology dependent?
We want to look at the closed dynamically triangulated random surfaces without self-avoidance. As models for such surfaces we take the first two topologically closed surfaces: The sphere and the torus (c.f. Figure 3.7). The torus is specified by identifying edges of the parameter space $\mathcal{P}$.

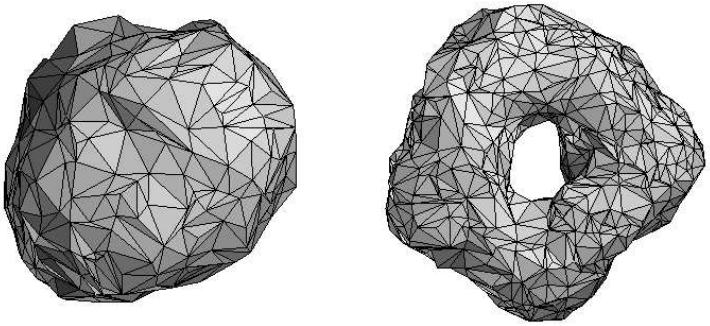

Figure 3.7: *Shown are two examples of configurations of dynamically triangulated random surfaces. The left picture shows a sphere and the right part a torus.*

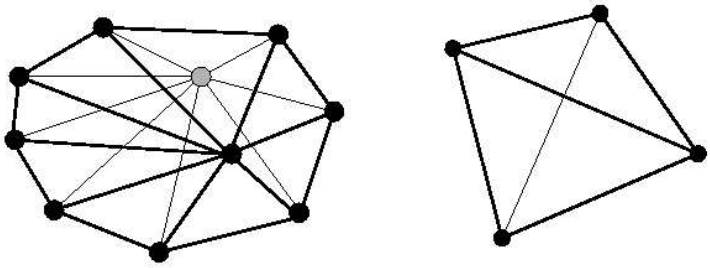

Figure 3.8: *This figure demonstrates the elementary moves which are made for dynamically triangulated random surfaces.*

Finite size scaling assumes, that there is only one relevant linear length scale, which is compared to the correlation length. To apply finite size scaling to the crumpling transition of dynamically triangulated random surfaces (DTRS) one must therefore assume a single length scale determined by the number of nodes N and the internal dimension d of the surface

$$L \propto N^{1/d} \quad . \tag{3.12}$$

This internal dimension d also depends on the external properties of the surface and λ [142].
So let us first look at the specific heat. If the transition is of second order we would have

$$C(\lambda, L) = L^{\alpha/\nu} \hat{C} \left[(\lambda - \lambda_c) L^{-\nu} \right] \tag{3.13}$$

where $\hat{C}$ is a scaling function, which depends on how one implements the surface. At the critical λ the scaling function is regular and the scaling hypothese leads to

$$C_N^{max} \propto A N^{\alpha/\nu d} + \ldots \tag{3.14}$$

for the scaling of the peak in the specific heat. If we assume a first order transition then C_N^{max} diverges as L^d because of the δ-distribution of $C_\infty(T)$ [173, 174, 172]. An evaluation of the specific heat C of DTRS (neglecting the metric contribution $\mathcal{H}_m$) gives the following expression

$$C_{all} = \frac{D}{2} + \frac{\lambda^2}{N} (< \mathcal{H}_e^2 > - < \mathcal{H}_e >^2) \quad . \tag{3.15}$$

The first part is related to the Gaussian Hamiltonian $\mathcal{H}_g$ and the second to the specific heat C of the edge extrinsic curvature $\mathcal{H}_e$. The specific heat for the edge extrinsic curvature is shown in Figure 3.9 for the two topologies considered. The interpolation was done by the method of Ferrenberg and Swendsen [183, 147] using histograms of $\mathcal{H}_e$.
Using the data of the specfic heat obtained by applying the extrapolation method, we can get a very accurate estimate of the positions of the maxima and of the heights. Figure 3.10 shows C_N^{max} of the torus and the sphere. A change to L^d behaviour is very unlikely and for that reason the data strongly suggest a continuous

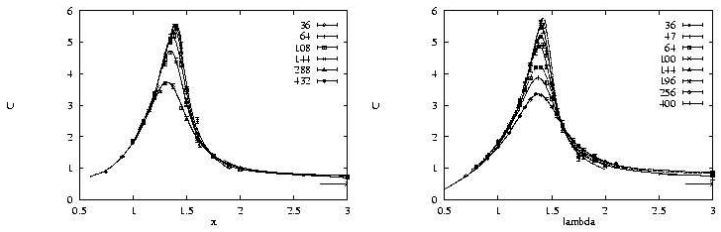

Figure 3.9: *Specific heat C (edge extrinsic curvature part) of the sphere (left part) and of the torus (right part).*

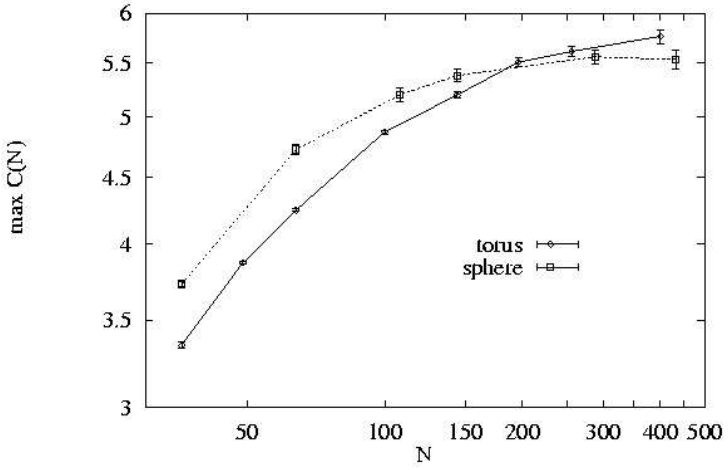

Figure 3.10: *Maximum of the specific heat C_N^{max} of the torus ($\Diamond$) and the sphere ($\Box$)*

phase transition in agreement with previous work [118, 124, 125, 126, 127, 148, 149].
From the data shown in Figure 3.10 we can obtain the following upper boundaries of critical exponents

$$\text{Sphere:}\frac{\alpha}{\nu d} \leq 0.00 \pm 0.04 \quad \text{Torus:}\frac{\alpha}{\nu d} \leq 0.06 \pm 0.02 \tag{3.16}$$

Using this simple method, we cannot distinguish a diverging specific heat with very small but positiv α, a logarithmic divergence $\alpha_s = 0$ and a power law cusp $\alpha_s < 0$, where α_s denotes the exponent of the singular part of the specific heat. We will use the abbreviation α instead of α_s.
Following Fisher [150], these three cases may be distinguished with a fit of the form

$$C(\Delta\lambda) = A \cdot \frac{1}{\alpha}\left(\Delta\lambda^{-\alpha} - 1\right) + B \quad , \quad \Delta\lambda = \left|\lambda_c^N - \lambda\right| \tag{3.17}$$

Figure 3.11 shows such fits for $\alpha = 0.1$ (power law), $\alpha = -0.01$ (near logarithmic) and $\alpha = -1.2, -2.0$ (power law cusp). The fits clearly favour a power law cusp of the specific heat with a large negative value of α, although we were not able to estimate the exponent α precisely.
Another possibility to determine the order of the transition is the cumulant $\mathcal{V}_N$ of the edge extrinsic curvature

$$\mathcal{V}_N := 1 - \frac{1}{3}\frac{\langle {\mathcal{H}_e}^4 \rangle_N}{\langle {\mathcal{H}_e}^2 \rangle_N^2} \, , \tag{3.18}$$

which behaves quite differently at temperature driven first- and second-order transitions [173, 174] :

$$\text{1. and 2.order:} \qquad \mathcal{V}_N|_{min} \overset{N\to\infty}{=} \tfrac{2}{3} \qquad T \neq T_c \text{fixed} \tag{3.19}$$

$$\text{2.order:} \qquad \mathcal{V}_N|_{min} \overset{N\to\infty}{=} \tfrac{2}{3} \qquad T = T_c(N) \tag{3.20}$$

$$\text{1.order:} \qquad \mathcal{V}_N|_{min} \overset{N\to\infty}{=} 1 - \frac{2\left(E_+^4 + E_-^4\right)}{3\left(E_+^2 + E_-^2\right)^2} \qquad T = T_c(N) \tag{3.21}$$

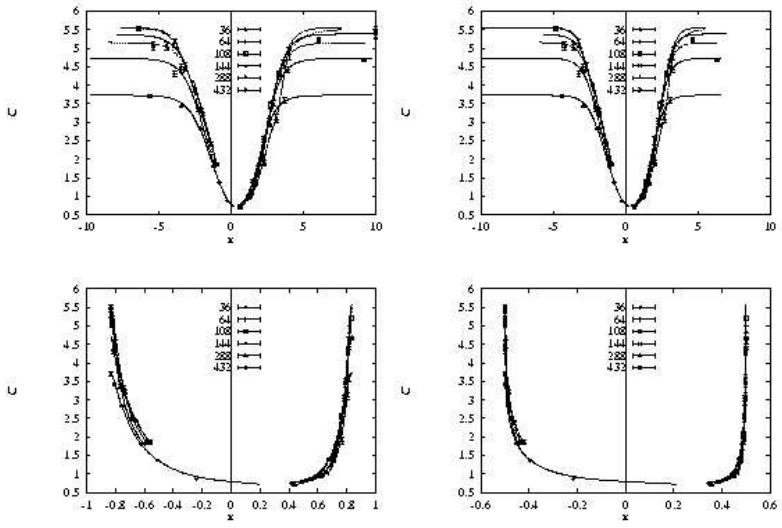

Figure 3.11: *Plot of the specific heat C against $x = \frac{1}{\alpha}\left(\Delta\lambda^{-\alpha} - 1\right)$ with $\alpha = 0.1$ (upper left), -0.01 (upper right), -1.2 (lower left) and $\alpha = -2.0$ (lower right).*

E_+ and E_- are the energies of the system above and below the transition. For a very weak first-order transition ($E_+ \approx E_-$) we also have $\mathcal{V}_N|_{min} \approx 2/3$.
We computed $\mathcal{V}_N$ defined by equation (3.18) using again the method of Ferrenberg and Swendsen [183, 147]. The resulting figures show the predicted single peak minima with wings following equation (3.19). The finite size dependence of the minima of $\mathcal{V}_N|_{min}$ shown in Figure 3.12 distinctly favours the asymptotic behaviour in equation (3.20) and therefore a continuous phase transition or a very weak first order transition.
In general, finite size scaling predicts also a shift $\Delta\lambda = \lambda_c^N - \lambda_c^\infty$ of the effective transition 'temperature' λ_c^N proportional to $N^{-1}(= L^{-d})$ for a first- and proportional to $N^{-1/\nu d}(= L^{-1/\nu})$ for a second-order transition. Unfortunatly λ_c^∞ of dynamically triangulated random surfaces is not known. For that reason, we have to use a two-parameter fit with unknowns λ_c^∞ and νd. But we can improve the reliability of this fit, because we know more. First, the fit has to be a straight line (neglecting corrections to scaling) and we have $\lim_{N\to\infty} \Delta\lambda(N) = 0$. Second, the shift $\Delta\lambda(N)$ is different for the specific heat and the cumulant in general. Therefore the slope of the fitted lines will be different in general, but we still have

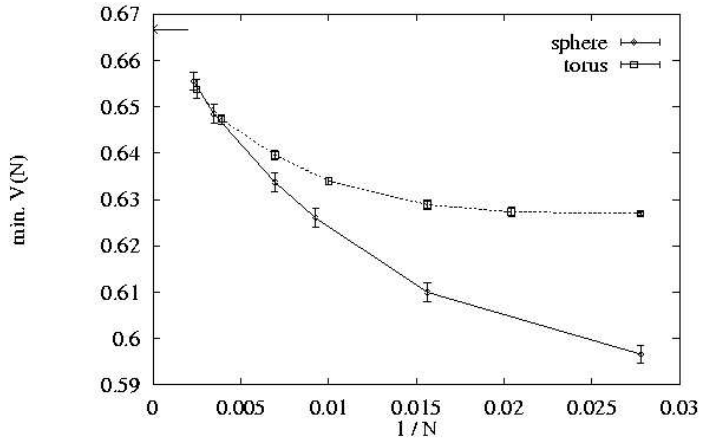

Figure 3.12: *Finite size dependence of the minimum $\mathcal{V}_N|_{min}$ of the reduced cumulant of the edge extrinsic curvature. $(\Diamond)$ denotes data of the sphere, $(\Box)$ those of the torus and the arrow the large N limit $2/3$ of a continuous transition.*

$\lim_{N\to\infty} \Delta\lambda(N) = 0$ for both observables.
Figure 3.13 shows the best fits for the sphere and the torus. The estimates of the parameters are

$$\lambda_c^\infty = 1.51 \pm 0.04 \quad , \quad \nu d = 3.2 \pm 0.5 \tag{3.22}$$

for the sphere and

$$\lambda_c^\infty = 1.47 \pm 0.02 \quad , \quad \nu d = 2.5 \pm 0.5 \tag{3.23}$$

for the torus.

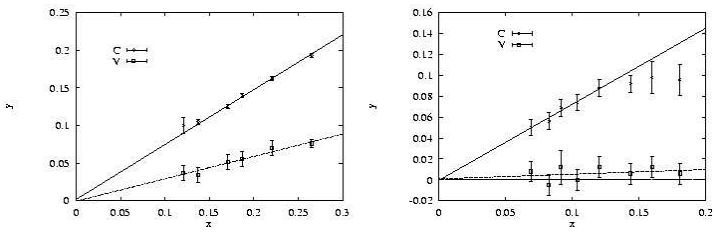

Figure 3.13: *Best fit of $y = \Delta\lambda$ against $x = N^{-1/\nu d}$ for the sphere (left part) and the torus (right part). $(\Diamond)$ denotes the specific heat C data, $(\Box)$ those of the cumulant $\mathcal{V}$.*

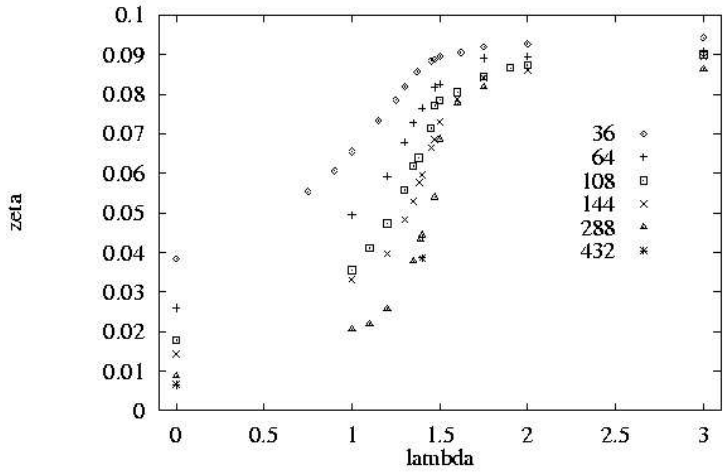

Figure 3.14: *Order parameter $\zeta = R^2/N$ of the sphere. Errors are smaller than symbol size.*

We turn now to the order parameter itself. Common practise is to take $\zeta = R/L$ (R is the typical radius, L the linear size of the membrane) to be a suitable order parameter [169, 159, 153, 154, 155, 156, 157]. Initially [157] it was also defined as $R_g(L) = \zeta L$ ($L \to \infty$), with the linear size L of the hexagon and the radius of gyration $R_g^2 \propto \sum_{ij} \left\langle |X_i - X_j|^2 \right\rangle$. A suitable choice for the order parameter therefore is

$$\zeta := R^2/N \tag{3.24}$$

with

$$R^2 = \frac{1}{N(N-1)} \left\langle \sum_{i,j}^{N} \sigma_i \sigma_j (\vec{X}_i - \vec{X}_j)^2 \right\rangle \tag{3.25}$$

σ_i denotes the number of nearest neighbours, i.e. the number of links connected to a node i. The associated susceptibility is

$$\chi_{R^2} := L^d \left(\langle \zeta^2 \rangle - \langle \zeta \rangle^2 \right) = \frac{1}{N} \left(\langle R^4 \rangle - \langle R^2 \rangle^2 \right)$$

Figure 3.14 shows the order parameter ζ and Figure 3.15 the susceptibilty of the sphere. The results for the torus are similar.

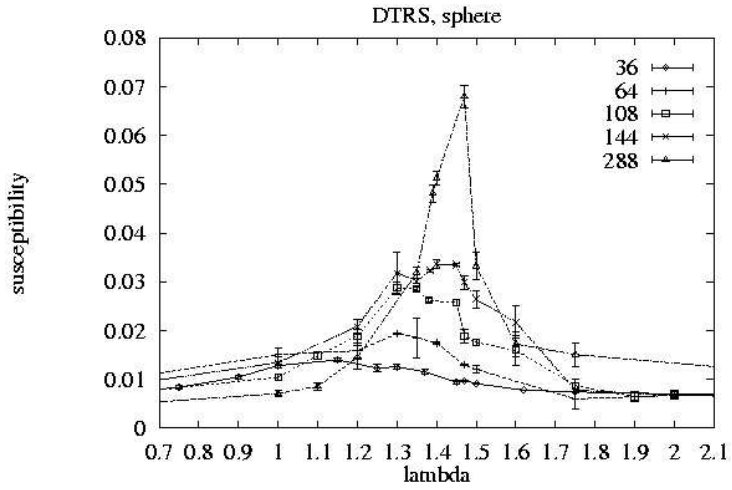

Figure 3.15: *Susceptibility χ_{R^2} of the sphere (Lines to guide the eye).*

Another possible order paramter $\zeta' = \langle R'^2 \rangle / N$,

$$\langle R'^2 \rangle = \frac{1}{N} \left\langle \sum_i^N \left(\vec{X}_i - \overline{\vec{X}} \right)^2 \right\rangle$$

which exhibits a small increase near the phase transition and a slower decay of ζ' for $\lambda \rightarrow 0$. The difference is caused by a change of the internal geometry near the phase transition [142].

With the data for the sphere in Figure 3.14 and the corresponding data of the torus one can estimate the critical exponent $\beta/\nu d$ of the order parameter assuming a second order transition. Here we use as the effective critical temperature the position of the peak of the specific heat. C^{max} (c.f. Figure 3.16).

An estimate of $\beta/\nu d$ using

$$\langle R^2(N, \lambda_c^{eff}) \rangle \propto N^{\beta/(\nu d)\ +\ 1} \tag{3.26}$$

results in

$$\text{Torus: } \beta/\nu d = 0.28 \pm 0.02 \ \ , \ \ \text{Sphere: } \beta/\nu d = 0.35 \pm 0.04 \tag{3.27}$$

and with the values of νd in equation (3.22) and (3.23)

$$\text{Torus: } \beta = 0.7 \pm 0.2 \ \ , \ \ \text{Sphere: } \beta = 1.1 \pm 0.2 \tag{3.28}$$

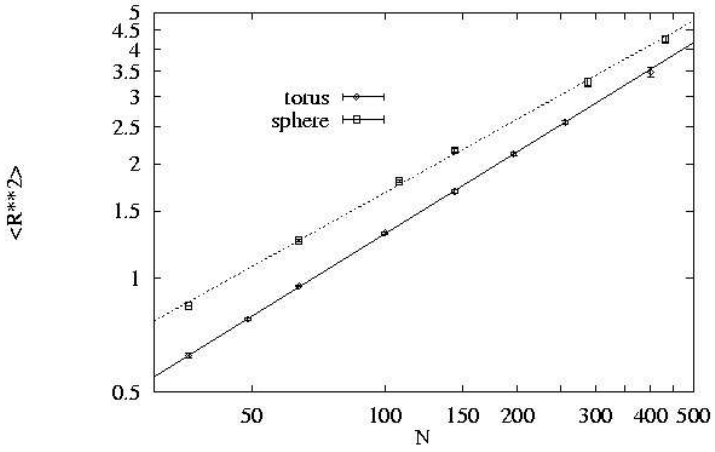

Figure 3.16: *Scaling of the radius of gyration squared $\langle R^2(N)\rangle$ at the position of the maximum of the specific heat C^{max}. $(\Diamond)$ denotes the data of the torus, $(\Box)$ data of the sphere.*

Figure 3.17 shows the scaling of the maxima of the susceptiblity χ (equation (3.26), Figure 3.15).
The results are

$$\text{Torus: } \gamma/\nu d = 0.62 \pm 0.06 \ , \quad \text{Sphere: } \gamma/\nu d = 0.66 \pm 0.06 \tag{3.29}$$

and, using the values of νd in equation (3.22) and (3.23),

$$\text{Torus: } \gamma = 1.6 \pm 0.5 \ , \quad \text{Sphere: } \gamma = 2.1 \pm 0.5 \ . \tag{3.30}$$

With these large error bars and estimated values $\alpha \approx -1.5$ the results are almost compatible with the scaling relation

$$\alpha + 2\beta + \gamma = 2 \tag{3.31}$$

3.1.3 Membranes and Folding

In the absence of self-avoidance, polymerized [162] and fluid [163] membranes adopt a crumpled random structure. Theoretical predictions by Flory mean-field approximation and Monte Carlo simulations [162] and renormalization group studies [164] supported the existence of a high temperature crumpled phase for

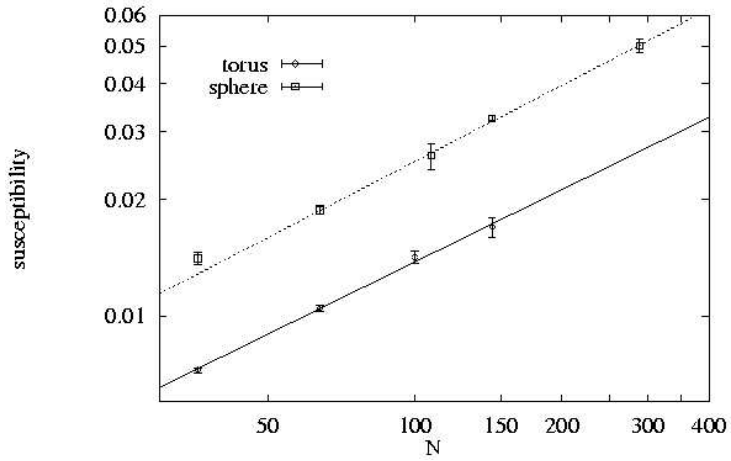

Figure 3.17: *Scaling of the susceptibility χ (equation (3.26), Fig. 3.15) in the case of a torus ($\Diamond$) and a sphere ($\Box$).*

self-avoiding polymerized membranes also, suggesting a possible finite temperature crumpling transition in the presence of an explicit bending rigidity [165]. However, more extensive computer simulations [159, 166, 167, 168] found no crumpling of self-avoiding tethered membranes in a good solvent. This prediction was confirmed by experimental studies of graphitic oxide [160].

On the other hand, polymerized vesicles undergo a wrinkling transition [161], and upon addition of 10 vol % acetone, Spector and co-workers [160] found small compact objects, which appeared to be folded. A poor solvent leads to (short-ranged) attractive interactions, and a single membrane was found to be flat for high temperatures [166], but in a collapsed state for sufficiently low temperatures [159]. The transition between the flat and the collapsed states of the membrane proceeds through a sequence of *folding transitions*, which were first found by cooling of a single membrane from the flat phase [169]. Because no hysteresis was found, it was ruled out that the folded configurations are metastable states. However, this method does *not* give sufficient evidence of the order or even the existence of a transition. For instance, hysteresis can also be found at *second order* phase transitions of finite systems and the results for one system size may be misleading. In addition, the experimentally observed wrinkling transition is first order [161].

Besides the nearest neighbour interactions, the membranes can be modeled similar to those of Abraham and Kardar [169]. The N particles of the polymerized membrane form the sites of a hexagonal shaped triangular lattice. The bond potential between nearest neighbour particles is

$$V^{\text{B}} = \sum_{j(i)} \left(b_0 - r_{ij}\right)^2 \quad , \tag{3.32}$$

with an equilibrium length b_0 and distances r_{ij} between particle i and its nearest neighbors $j(i)$. In place of this harmonic potential, tethers were used by Abraham and Kardar [169].

All particles interact through a shifted Lennard-Jones potential

$$V_{ij}^{\text{LJ}} = \begin{cases} \left(\frac{1}{r_{ij}^{12}} - 2\frac{1}{r_{ij}^{6}}\right) + \left(\frac{1}{r_c^{12}} - 2\frac{1}{r_c^{6}}\right) & , \quad r_{ij} <= r_c \\ 0 & , \quad r_c < r_{ij} \end{cases} \tag{3.33}$$

with a cut-off at $r_c = 2.5$. The repulsive part of this interaction guarantees self-avoidance of the membrane.

The folding of the membrane can be described by the eigenvalues ${\lambda_1}^2 >= {\lambda_2}^2 >= {\lambda_3}^2$ of the inertia tensor

$$\mathcal{T}_{\alpha,\beta} = \frac{1}{N} \sum_{i=1}^{N} \left(r_{i\alpha} r_{i\beta} - \overline{r}_\alpha \overline{r}_\beta\right) \quad , \tag{3.34}$$

where $\alpha, \beta \in \{x, y, z\}$, and the sum runs over all particles of a given configuration; $\overline{r}_\alpha$ is the α component of the center of mass for a configuration. We can estimate the expected change of the membrane eigenvalues by those of an unfolded or folded disc with radius 1 and width $d = 0.1$ as shown in Table 3.1. Taking into account all three eigenvalues, an unfolded, folded or twice folded configuration can be distinguished. A collapsed configuration would be indicated by approximately equal eigenvalues.

At the first folding transition, the eigenvalue λ_1^2 stays constant approximately, while the second eigenvalue λ_2^2 decreases by a factor $c \approx 0.2790$. Therefore, we define an *order parameter* m by

$$\langle m(\beta) \rangle = \left\langle \frac{1}{(1-\sqrt{c})} \left[\frac{\lambda_2(\beta)}{\lambda_2(\beta_0)} - \sqrt{c} \right] \right\rangle \quad , \tag{3.35}$$

configuration	${\lambda_1}^2$	${\lambda_2}^2$	${\lambda_3}^2$
disc	0.2543	0.2473	0.00084
disc, folded	0.2524	0.0690	0.00332
disc, folded twice	0.0929	0.0487	0.01330
disc	1.0000	1.0000	1.00
disc, folded	0.9925	0.2790	3.95
disc, folded twice	0.3653	0.1969	15.83

Table 3.1: Eigenvalues of the moment of inertia tensor of a disc with radius 1 and width $d = 0.1$. In the lower part, all numbers are relative to the values of the unfolded disc.

where $\lambda_2(\beta_0)$ is a reference value of an unfolded membrane at β_0 far below the inverse critical temperature β_c. At a first order transition, the average order-parameter discontinuously jumps at β_c [172, 173, 174]. Contrary, at a continuous phase transition we expect a power law behavior of the average order parameter $\langle m \rangle(\beta)$ with an exponent β', i.e. $\langle m \rangle \propto (\beta - \beta_c)^{\beta'}, \beta > \beta_c$ [175, 176, 177, 178]. Indeed, the average order parameter $\langle m \rangle$ becomes very steep near β_c with increasing number of particles N (data not shown). In principle, one can measure the increase of the slope and compare to the predictions of finite size scaling theory. Of course, the slope of $\langle m \rangle(\beta)$ is proportional to the *susceptibility* χ, which can be measured by the fluctuations of m also:

$$\chi(\beta) = L^d \beta \left(\langle m^2 \rangle_L - \langle m \rangle_L^2 \right) \tag{3.36}$$

The susceptibility $\chi(\beta)$ is shown in Figure 3.18 and the scaling of the maximum $\max \chi(\beta)$ in the inset of Figure 3.18.
At a first order transition, $\chi(\beta_c^{\text{eff}})$ is expected to increase proportional to $N = L^d$ [172, 173, 174]. At a continuous phase transition, $|\beta - \beta_c|^{-\gamma_\pm}$ is predicted [175, 176, 177, 178]. The L^d increase of $\chi(\beta)$ in Figure 3.18 gives evidence of the scaling at a *first order* transition. In addition, the width of the susceptibility peak should decrease as L^{-d} [172, 173, 174]. Figure 3.19 shows a finite size scaling plot of the susceptibility data. Within errors, *first order* scaling behavior can be observed, at least above the inverse transition temperature.
The transition temperature β_c^∞ can be extrapolated by the position of the max-

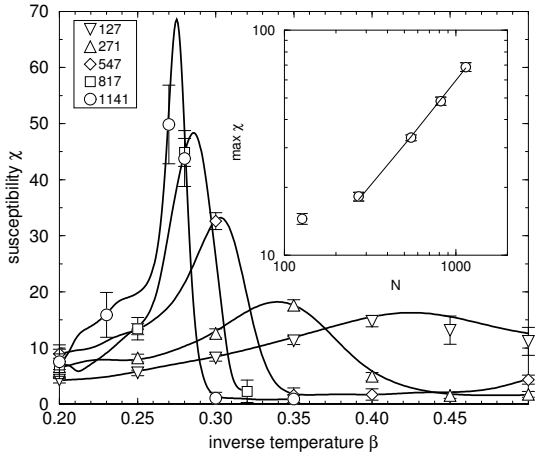

Figure 3.18: Susceptibility $\chi(\beta)$ for membranes with $N = 127, 271, 547, 817$ and 1141 particles. The solid lines were computed by the multi-histogram method. The scaling of the maximum $\max \chi$ is shown in the inset.

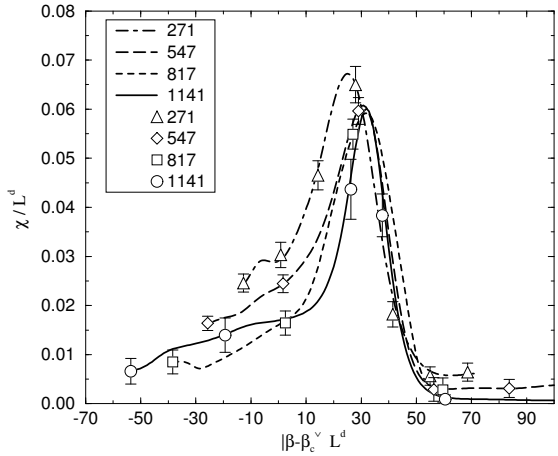

Figure 3.19: Finite size scaling plot of the susceptibility $\chi(\beta)$ for a first order transition using the value $\beta_c^\infty = 0.247(5)$ from Figure 3.20.

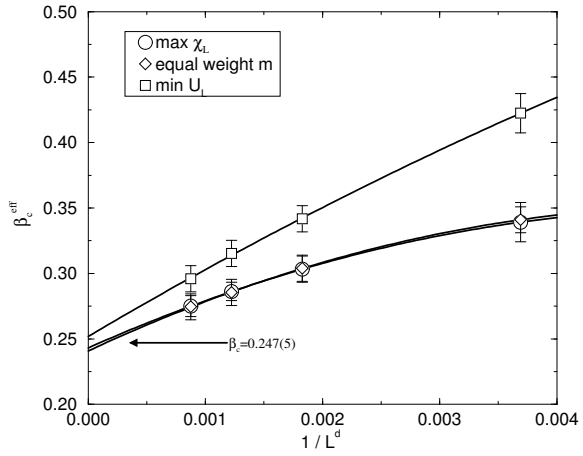

Figure 3.20: Critical temperature $\beta_c^\infty = 0.247(5)$ determined by the position of the maximal susceptibility χ, the minimum of the cumulant U_L and equal-weight of the order parameter distribution for the four largest system sizes.

imum in $\chi(\beta)$ [174], the minimum of the cumulant [174] and the equal weight criterion [180] of the order parameter distribution. At least for χ, the equal weight criterion predicts a shift of the effective transition temperature proportional to L^{-2d} [179, 180, 181], whereas a shift proportional to $\propto L^{-1/\nu}$ is expected for a continuous phase transition. Using quadratic terms in the regression, the extrapolations in Figure 3.20 of the three observables agree within errors. The transition temperature of the first folding transition is found to be $\beta_c^\infty = 0.247(5)$.

The increase of the susceptibility is caused by the characteristic double-peak structure of the order parameter distribution near β_c, which is typical for a discontinuous phase transition [172, 173, 174, 175, 179, 180, 181, 182]. Figure 3.21 shows the expected double-peak distribution $P(m)$ at the equal height transition temperature [180]. The development of a minimum in $P(m)$ is confirmed by the method of Lee and Kosterlitz [182]. The measured ΔF in the inset of Figure 3.21 is proportional to the free energy difference at the equal height transition temperature and increases as $\left(L^d\right)^x$, $x{\approx}1.3$.

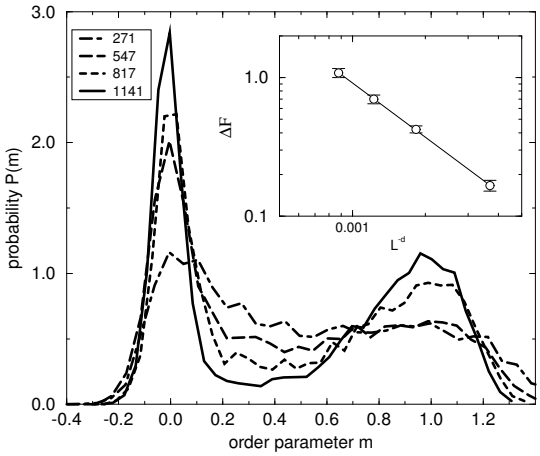

Figure 3.21: Probability distribution $P(m, \beta_{ew})$ of the order parameter m at the equal-weight transition temperature β_{ew}. The inset shows the free energy difference ΔF at the equal-height transition temperature β_{eh}, which increases $\propto (L^d)^x$, $x \approx 1.3$.

Further, $P(m)$ can be described by the reduced cumulant U_L

$$U_L(\beta) = 1 - \frac{\langle m^4 \rangle_L}{3\langle m^2 \rangle_L^2} \quad . \tag{3.37}$$

At a continuous phase transition, $U_L(\beta)$ is expected to approach $2/3$ for all β. The data shows a minimum, which becomes more pronounced for large N, indicating a *first order* phase transition (figure not shown).

The folding of the membrane must be visible in the attractive part of the potential energy, also. In fact, there is a jump in the potential energy and the related specific heat develops a peak, although very slowly. Besides the above defined order parameter, which is based on the geometry of the membrane, we can derive a different order parameter from the attractive part of the Lennard-Jones potential:

$$\tilde{m} = \frac{1}{N} \left\{ \sum_{i<j} \Theta\left(r_c - r_{ij}\right) \left(2\frac{1}{r_{ij}^6} + 2\frac{1}{r_c^6} \right) \right\} \quad . \tag{3.38}$$

Compared to m, the order parameter $\tilde{m}$ has the advantage, that it is a local property. We performed *Hybrid Monte Carlo* simulations with an additional term

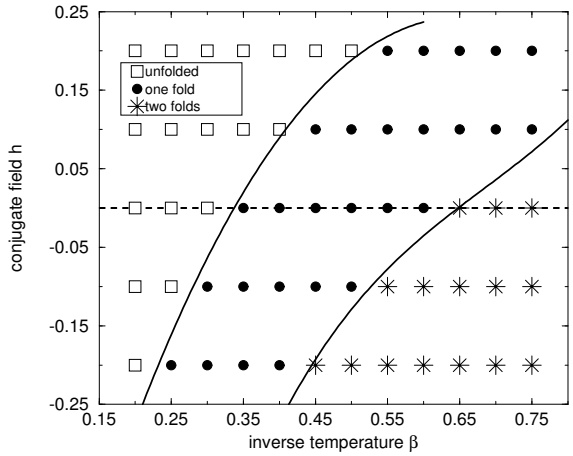

Figure 3.22: Phase diagram of a membrane with 271 particles in the β, h plane. The symbols denote the result of the simulations, the solid lines are the first order transition lines computed by the multi-histogram method.

$h \cdot \tilde{m}$ in the Hamiltonian, where h is the conjugate field. Figure 3.22 shows the phase diagram in the (β, h)-plane of a membrane with 271 particles. The first order transition lines were computed by the multi-histogram method [183]. For the transition from one to two folds, an order parameter similar to m is used, which is based on λ_1 instead of λ_2. $h = 1$ is an upper limit for both transition lines, because of the vanishing attractive interactions at $h = 1$.

The unfolding of a singly folded membrane bears close resemblance to the unbinding transition of two distinct surfaces. Regarding a folded membrane of N particles, the fraction of particles near the crease decreases with $1/\sqrt{N}$. Therefore, the nature of the folding transition is related to the nature of the underlying unbinding transition of two distinct membranes without the crease. The shape fluctuations of a single membrane of lateral size $\xi_\parallel$ are characterized by the typical fluctuation amplitude $\xi_\perp \propto {\xi_\parallel}^\zeta$. Polymerized membranes without lateral tension have a roughness exponent $\zeta \approx 0.6$. The steric hindrance of two interacting membranes at separation l leads to an overall loss of entropy, which can be regarded as an effective fluctuation-induced repulsion, $V_{rep} \propto 1/l^\tau$ with decay

exponent $\tau \approx 3.3$ for polymerized membranes. This repulsive interaction causes the unfolding of the membrane even in the presence of attractive van der Waals interactions. However, the crease of the folded membrane introduces an additional attractive interaction. This situation is similar to a membrane interaction which exhibits two minima at two different separations. Such an interaction implies a *first-order* unbinding transition [185] and may be an explanation of the *first-order* folding transition.